nature COMMUNICATIONS

ARTICLE

Received 18 Jul 2014 | Accepted 21 Jan 2015 | Published 27 Feb 2015

DOI: 10.1038/ncomms7344 OPEN

North Atlantic storm track changes during the Last Glacial Maximum recorded by Alpine speleothems

Marc Luetscher[1,2], R. Boch[1,3], H. Sodemann[4,5], C. Spötl[1], H. Cheng[6,7], R.L. Edwards[7], S. Frisia[8], F. Hof[9] & W. Müller[10]

The European Alps are an effective barrier for meridional moisture transport and are thus uniquely placed to record shifts in the North Atlantic storm track pattern associated with the waxing and waning of Late-Pleistocene Northern Hemisphere ice sheets. The lack of well-dated terrestrial proxy records spanning this time period, however, renders the reconstruction of past atmospheric patterns difficult. Here we present a precisely dated, continuous terrestrial record of meteoric precipitation in Europe between 30 and 14.7 ka. In contrast to present-day conditions, our speleothem data provide strong evidence for preferential advection of moisture from the South across the Alps supporting a southward shift of the storm track during the local Last Glacial Maximum (that is, 26.5–23.5 ka). Moreover, our age control indicates that this circulation pattern preceded the Northern Hemisphere precession maximum by ~3 ka, suggesting that obliquity may have played a considerable role in the Alpine ice aggradation.

[1] Institute of Geology, University of Innsbruck, Innsbruck 6020, Austria. [2] Swiss Institute of Speleology and Karst Studies—SISKA, 2301 La Chaux-de-Fonds, Switzerland. [3] Institute of Applied Geosciences, Graz University of Technology, 8010 Graz, Austria. [4] Institute for Atmospheric and Climate Science, ETH, 8092 Zurich, Switzerland. [5] Geophysical Institute, University of Bergen, 5020 Bergen, Norway. [6] Institute of Global Environmental Change, Xi'an Jiaotong University, Xi'an 710049, China. [7] Department of Earth Sciences, University of Minnesota, Minneapolis, 55455 Minnesota, USA. [8] School of Environmental and Life Sciences, University of Newcastle, Callaghan, NSW 2308, Australia. [9] Swiss Society of Speleology, 2301 La Chaux-de-Fonds, Switzerland. [10] Department of Earth Sciences, Royal Holloway University of London, Egham TW20 0EX, UK. Correspondence and requests for materials should be addressed to M.L. (email: marc.luetscher@uibk.ac.at).

The Last Glacial Maximum (LGM) characterizes the climax of a pronounced sea-level minimum associated with the global ice extent during the Upper Pleistocene, between ca 26.5 and 19 ka (refs 1,2). While atmospheric circulation models support a southward shift of the North Atlantic storm tracks to ~40 °N (refs 3,4) paleoclimate proxy records point to a global mean temperature decrease of between 4 and 7 °C when compared with preindustrial times[5]. In the European Alps, the extent of the regional ice sheet has been comprehensively documented by detailed geomorphological mapping[6,7]. Observations of trimlines reveal the presence of three major ice domes, all located south of the present climate divide, suggesting that precipitation was mostly associated with air advection from the South[8]. However, in the absence of continuous terrestrial palaeoclimate records from the northern Alpine mountain chain, it is yet unclear whether this precipitation pattern was associated with increased cyclogenesis in the western Mediterranean[9] or if it relates to an overall shift in the storm trajectories from the eastern North Atlantic[8]. This uncertainty in regional atmospheric circulation patterns has major implications, primarily for the regional ice build-up and thus the timing of valley glacier advances but also for the distribution of temperature and precipitation responses and thus implicitly also for vegetation refugia.

Reconstructing LGM atmospheric circulation in the European Alps remains inherently difficult and requires accurately dated high-resolution climate proxy records. High-altitude ice cores certainly represent the most direct precipitation archive at mid-latitudes, but barely cover the Holocene[10]. Ice and permafrost conditions in the Alpine foreland further hinder formation/preservation of possible lake records and biogenic proxies during the LGM. Speleothems, secondary carbonate deposits found in caves, represent an alternative archive for Late Pleistocene climate history provided that the temperature in the subsurface stayed above freezing and local water–rock interactions gave rise to calcite-supersaturated water.

Here we present the first continuous continental European record of meteoric precipitation obtained from speleothems grown during Marine Isotope Stage 2. We show that our record reflects atmospheric circulation patterns in the Northern Hemisphere during the LGM, supporting a southward shift of the North Atlantic storm track about 3 ka before the precession maximum. We conclude that the preferential advection of moisture from the South likely favoured regional differences in the ice build-up in the Alps, which suggests contrasting responses of valley glacier advances during the LGM.

Results

Study site. Two coeval speleothems (7H-2 and 7H-3) were sampled in the Sieben Hengste (7H) cave system (Bernese Alps, Switzerland; Fig. 1), a network comprising more than 150 km of explored cave passages. The galleries formed within Urgonian carbonates (Schrattenkalk Formation), which are locally overlain by low-permeable Eocene sandstones (Supplementary Fig. 1). Several lines of evidence, including alignments of erratic boulders and glacial striations, point to an ice-covered hydrological catchment at 1,700–2,000 m a.s.l. during the LGM[7]. Based on geomorphological evidence from the nearby Napf palaeoglacier, the local Equilibrium Line Altitude (ELA) during the LGM is estimated at ca 1,250 m a.s.l. Despite the low temperatures expected during the LGM, summer rainfall and seasonal melting of winter-snow must have been sufficient to allow for recharge into the Sieben Hengste karst system and ensure speleothem deposition. Concentrated infiltration along major tectonic discontinuities likely maintained a locally constant temperature boundary condition in the epikarst close to the melting point (that is, 0 °C), whereas hydrological drainage ensured geothermal heat advection off the phreatic zone. Accordingly, the vertical temperature distribution in the Sieben Hengste karst system most likely followed the adiabatic lapse rate of humid air[11], implying an isotherm of ca 1.0 ± 0.5 °C at 1,500 m a.s.l.

Speleothem samples. The two stalagmites (Supplementary Fig. 2) were collected ca 215 m below the ground surface (that is, 1,540 m a.s.l.) in an alcove at the base of a vadose shaft. The candle-shaped stalagmites, 57- and 30-cm long show similar petrographies dominated by bundles of elongated columnar fascicular optic calcite crystals, commonly arranged in fans (Supplementary Fig. 3). This fabric is typical of elevated Mg/Ca ratios in the drip water and agrees with the chemical concentrations measured in the speleothem (Supplementary Table 1). Both, the calcite fabrics

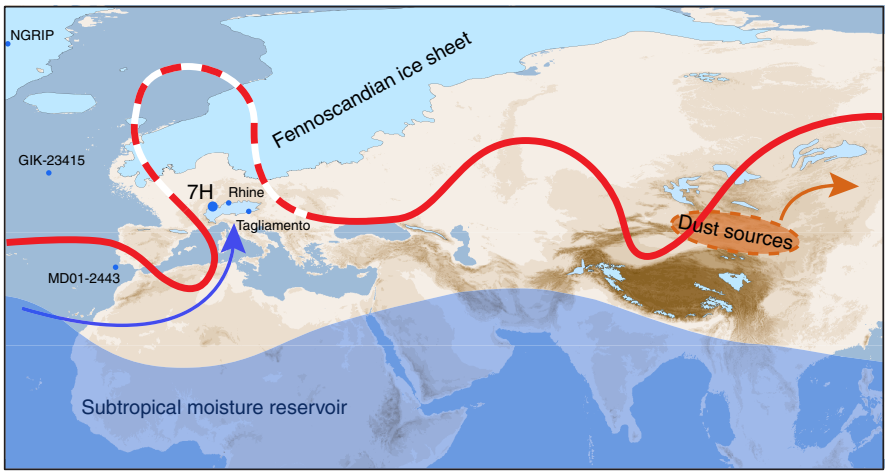

Figure 1 | Sieben Hengste site location. Conceptual view of southerly moisture transport to the Alps during the Last Glacial Maximum (blue arrow) from the subtropical reservoir (blue shading). The advection of moisture is triggered by Rossby-wave breaking of the jet stream over Western Europe (red line), which is enhanced due to the presence of the Fennoscandian ice shield (light blue; 6) and the associated semi-permanent blocking high. Dust-mobilizing storms are induced further East by jet stream excursions propagating to Central and Eastern Asia (orange area and arrow). 7H: Sieben Hengste cave system; NGRIP: ice core; GIK-23415 and MD01-2443: deep sea sediment cores; Rhine and Tagliamento: palaeoglaciers.

and the regular stalagmite morphologies suggest that the karst aquifer properties remained constant over decadal to millennial timescales. The regular recharge was mainly controlled by the glacier hydrology. Hence, the temperature in the cave remained largely constant, and we surmise that the 7H $\delta^{18}O$ is primarily controlled by changes in the precipitation isotope composition.

The 7H-record. The 50 uranium-series ages obtained by multi-collector inductively coupled plasma mass spectrometry are all in stratigraphic order and reveal continuous calcite deposition from 30.0 to 14.7 ka b2k (Supplementary Table 2). Typical age uncertainties of less than 0.5% reflect the elevated ^{238}U concentration of $1,200 \pm 300\ ng\ g^{-1}$ associated with low detrital thorium contents. The age model reveals an average growth rate of 40–70 $\mu m\ a^{-1}$ (Supplementary Fig. 4). Sub-samples for $\delta^{18}O$ and $\delta^{13}C$ analyses were milled at 200 µm intervals along the speleothem growth axis providing an average resolution of 4.5 a.

The speleothem oxygen isotope composition (ca 4,200 analyses) ranges between $\delta^{18}O_{VPDB}$ −10.5 and −13.5‰ and oscillates on decadal to millennial time scales (Fig. 2b). The stalagmite $\delta^{18}O$ time series correlate in overlapping segments and, therefore, likely responded to the same hydrological forcing. This hydrological control is emphasized by a high local correlation ($r^2 = 0.54$) between $\delta^{18}O$ and $\delta^{13}C$, which suggests that any decrease in drip rate related to lower recharge forced a coherent C isotope change (Supplementary Fig. 5). Overall, $\delta^{13}C$ values stayed remarkably constant at $+4.4 \pm 0.4$‰, indicating that the dissolved inorganic carbon was largely derived from the host rock. A composite $\delta^{18}O$ record was obtained by using a Monte Carlo (MC) approach to find the best-possible correlation between adjacent time series (see Methods for details).

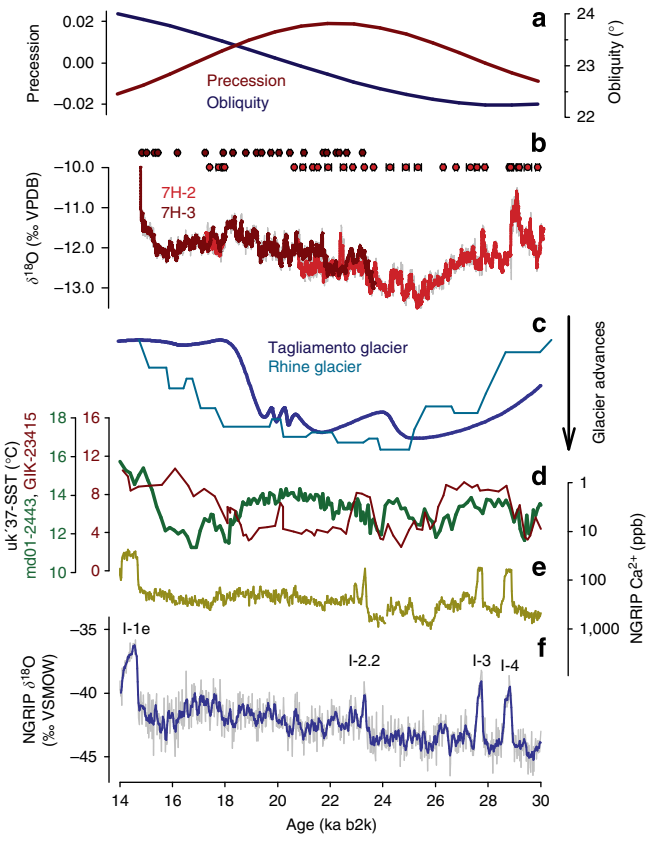

Figure 2 | LGM data comparison. (**a**) Precession (brown) and obliquity (blue)[23]. (**b**) 7H-2 (red) and 7H-3 (brown) $\delta^{18}O$ time series (21a low-pass filter) plotted with individual U/Th ages and measured errors (2σ). (**c**) Alpine glacier advances reconstructed for Tagliamento and Rhine glaciers[17,18]. (**d**) North-eastern Atlantic sea-surface temperature[15,16]. (**e**) NGRIP dust record[33]. (**f**) NGRIP $\delta^{18}O$ with a 100a low-pass filter[12].

Discussion

The 7H $\delta^{18}O$ record shows remarkable similarities to Northern Hemisphere palaeoclimate records, both at orbital and millennial timescales. Positive $\delta^{18}O$ excursions of 7H (Fig. 2b) match the North Greenland Ice Core Project (NGRIP) $\delta^{18}O$ record (Fig. 2f) for Interstadials (I) 3 and 4 within dating uncertainties[12,13] (Table 1). The timing of the rapid $\delta^{18}O$ increase at the onset of the Bølling (that is, I-1e at 14.70 ka) is identical with the timing in NGRIP and led to a stalagmite growth stop due to the waning of the glacier cover in the hydrological catchment of the cave system. We argue that the high degree of similarity between the 7H-record and Greenland ice cores reflects the common variability of the North Atlantic climate system[14]. This interpretation is supported by coeval changes in the sea-surface temperature recorded off the Iberian Peninsula[15] (core 2443 in Fig. 2d). This covariance is highest when the near-surface poleward heat transfer, between 26.3 and 23.5 ka, was strongly reduced[16](for example, core 23415 for comparison in Fig. 2d), suggesting internal feedback mechanisms associated with variations in the Atlantic Meridional Overturning Circulation.

In contrast to the NGRIP record, the 7H $\delta^{18}O$ record is characterized by an absolute minimum centred at ca 25.3 ka, consistent with the maximum Alpine glacier advance inferred from independently dated geomorphological field evidence[17,18] (Fig. 2c). In addition, second-order changes in the 7H $\delta^{18}O$ time-series correlate within dating uncertainty with minor glacier oscillations reconstructed from proglacial sediments[17] and agree with a perialpine vegetation record from Les Echets, eastern France[19], which has been interpreted to reflect primary changes in soil moisture availability. Based on these evidences, we surmise that the 7H $\delta^{18}O$ record mirrors changes in the mass balance of LGM glaciers in the Alps and thus predominantly reflects changes in the Alpine precipitation pattern[8].

The modern regime of moisture transport to Sieben Hengste is dominated by westerly advection (Supplementary Fig. 6), while about 10–30% of the annual precipitation is transported on average from the South across the Alpine mountain range. Intense southerly moisture advection is known to be related to pronounced Rossby-wave breaking west of the Alps, which induces enhanced meridional flow of moist and warm subtropical air towards the mountain range[20]. Such transport patterns may have been dominant during the LGM when both a larger (winter)

Table 1 | Comparison of event boundaries as determined in Greenland and their counterparts in 7H.

	Greenland[13]		7H	
	Age b2k	Maximum counting error	U/Th age b2k	Error 2σ
I-1e	14 692	186	14 708	± 40
S-2.1	22 900	573	22 809	± 47
I-2.1	23 020	583	22 938	± 50
S-2.2	23 220	590	23 021	± 46
I-2.2	23 340	596	23 280	± 37
S-3	27 540	822	27 686	± 65
I-3	27 780	832	27 854	± 54
S-4	28 600	887	28 706	± 64
I-4	28 900	898	29 109	± 66

An event is defined by the first clear signal deviating from the base line before the transition[13].

sea-ice cover in the North Atlantic[21] displaced the baroclinic zone further south and a semi-persistent blocking high over the Fennoscandian ice sheet deflected the North Atlantic jet stream substantially, leading to more frequent Rossby-wave breaking (Fig. 1). Since the tropics and subtropics experienced comparatively less temperature changes during glacial-interglacial cycles, the subtropical moisture reservoir could have provided sufficient moisture for precipitation to build up and maintain ice domes in the Alps with meridional moisture transport events. The strong correlation between the 7H-record and the Alpine ice mass balance (Fig. 2c) suggests that this atmospheric circulation pattern may have been a characteristic mechanism of moisture delivery to the Alps during the LGM.

Accordingly, we propose that, during the LGM, the isotopic composition of 7H primarily recorded changes in the position of the North Atlantic storm track and associated changes of moisture advection to the Alps. This hypothesis is generally consistent with global climate simulations suggesting an overall southward displacement of the storm track during the LGM[3,4], accompanied by a significant precipitation increase in the mid-latitudes, in particular around the Iberian Peninsula[21]. Meanwhile, reconstructed meridional temperature gradients based on Alpine glacier's ELA depression suggest cold and dry conditions in the northern Alps at the LGM climax[22]. The presence of liquid water in the 7H karst system at 1,750 m a.s.l., however, challenges an estimated mean annual air temperature of -10 to -15 °C at the ELA of glaciers[22] and suggests that major precipitation events must have been associated with substantial advection of warm moist air, predominantly between spring and autumn. Owing to their transient nature, such events are hardly reflected in the mean annual air temperature record[23] and the relatively small changes in the temperature of condensation only had a minor influence on the isotopic composition. Similarly, the extraordinarily cold and dry climate during the LGM makes it unlikely to explain the depletion in $\delta^{18}O_{cc}$ by a seasonal shift towards more winter precipitation. Instead, we propose that a higher fraction of precipitation was transported across the Alpine mountain range from the South because of a change in the predominant synoptic circulation pattern. The higher orographic barrier along the southerly transport path cause more moisture to condensate resulting in an orographically induced Rayleigh fractionation process (Supplementary Fig. 7). Accordingly, phases of more depleted $\delta^{18}O_{cc}$ are associated with the preferential advection of moisture from the South (see Supplementary Discussion), whereas less depleted $\delta^{18}O_{cc}$ values primarily reflect air masses reaching the northern Alps directly from the Northwest (Fig. 3). Based on the apparent correlation between the Remanzacco oscillations of the LGM South Alpine Tagliamento paleoglacier[17] and the 7H-record, the 50% threshold is assessed at $\delta^{18}O_{cc}$ -12.4 ± 0.1‰, which corresponds to ca -16.3‰ on the Vienna Standard Mean Ocean Water (VSMOW) scale (Fig. 4). Because $\delta^{18}O$ at the oceanic moisture source has not changed substantially during the LGM, a two end-member mixing model allows to derive that the contribution of moisture crossing the Alps may have varied between 25 and 65% during the LGM.

Associating the (Alpine) LGM with a change in the synoptic circulation pattern rather than an insolation minimum enables alternative interpretations for the causes of major glacier advances in the Alps. We note that the 7H $\delta^{18}O$ minimum predated the precession maximum at 22 ka (ref. 24) by ca 3 ka, suggesting a combined effect of precession and obliquity on the timing of the last Alpine glaciation, and thus possibly also on its global counterpart[25]. Evidence of de-phasing with respect to the precessional band has been reported from marine and terrestrial records[26], but interpretations were mainly focused on the timing of deglaciation. Although changes in obliquity influence the latitudinal distribution of solar radiation and thus control glacier ablation[27], its effect on ice accumulation is less obvious. Yet, the obliquity minimum at 29 ka (ref. 24) implies reduced energy input at high latitudes. The associated cooling of the Northern Hemisphere likely favoured a drop in the ELA, as exemplified by the start of speleothem growth at 7H at 30 ka. With tropical and subtropical areas being less affected by changes in obliquity, meridional temperature gradients and therefore also pressure gradients became steeper, strengthening the jet stream, which, together with an expansion of the Fennoscandian ice sheet, progressively migrated southwards[3]. This may have led to enhanced synoptic storm activity in North-Atlantic mid-latitudes, and possibly also in areas further downstream, because of jet stream excursions induced by the interaction between the jet and a quasi-stationary blocking over the Fennoscandian ice sheet (Fig. 1). The concomitant decline of the mid-latitude vegetation cover increased the potential global dust emissions by nearly 38% (ref. 28). An intriguing similarity is noted between the Ca record of NGRIP and the 7H $\delta^{18}O$ record (Fig. 2e), which is particularly pronounced between 28 and 23 ka (that is, $r \geq 0.60$ between 25.5 and 23.0 ka; Supplementary Fig. 8).

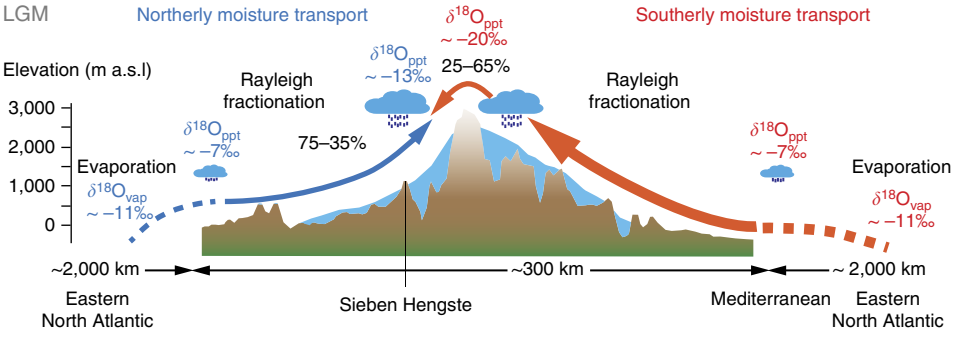

Figure 3 | Conceptual model of isotope fractionation in meteoric precipitation along two distinct trajectories. Rayleigh isotope fractionation along the northwestern (blue) and southern moisture transport trajectory (red) for the Last Glacial Maximum. Moisture evaporates from the source region in the Eastern North Atlantic and then follows a fractionation path with orographic rainout up to 1,700 m a.s.l. during northerly advection, or up to 3,000 m a.s.l. for the southerly advection across the Alpine main crest. $\delta^{18}O$ values are expressed in VSMOW. Percentages reflect the proportion of precipitation reaching 7H along the northwestern and southern routes, respectively. The ranges reflect uncertainties on the interannual variability (see Supplementary Discussion for details). Based on the 7H $\delta^{18}O$ record, we surmise that the proportion of North Atlantic moisture transported from the South to 7H during the LGM was two to three times higher than today.

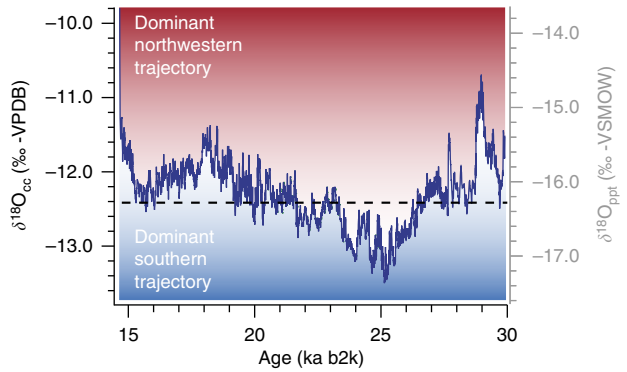

Figure 4 | The composite 7H $\delta^{18}O$ record. The correlation with the Alpine Tagliamento glacier advances[17] (Fig. 2c) suggests that low $\delta^{18}O$ values are primarily associated with moisture transport from the South. The stippled line marks the approximate equilibrium between northwestern and southern moisture transport as identified from the Remanzacco oscillations. A dominant northwestern trajectory reflects a more northerly storm track position, and vice-versa. The secondary *y* axis shows the inferred isotopic composition of meteoric precipitation assuming calcite precipitation close to thermodynamic equilibrium[34] in a cave environment just above freezing point.

Elevated dust concentrations in Greenland ice cores correlate with depleted $\delta^{18}O$ values in 7H. This increased dust mobilization during periods when the storm track was dominantly south of the Alps supports a potential teleconnection between North Atlantic moisture transport and storminess in East Asian regions (Supplementary Discussion). Concurrently, the preferential transport of moisture towards the southern flank of the Alps favoured snow accumulation in the glaciological catchment of the large piedmont glaciers. These results are not only consistent with independent geomorphological evidence[7,8] but also argue for a non-uniform ice build-up in the Alps during the LGM. Accordingly, we expect regional differences in the timing of valley glacier advances depending on the location of the glaciers' accumulation areas.

We conclude that the Alpine glaciers responded in a sensitive way to Northern Hemisphere atmospheric circulation patterns during the LGM. Therefore, this mountain range represents a key location for identifying large-scale atmospheric reorganizations in the North Atlantic climate systems. The importance of moisture advection towards the Alps for glacier advances calls for high-resolution GCM simulations of the LGM climate, which could be tested extensively using 7H as a benchmark.

Methods

U/Th dating and age modelling. Chemical separation and MC-ICP-MS (Thermo-Finnigan Neptune) measurements of U and Th isotopic ratios were undertaken at the University of Minnesota using procedures similar to those described in ref. 29. The extent of detrital ^{230}Th contamination was estimated and corrected for by measurement of the long-lived chemically equivalent ^{232}Th and assuming a silicate bulk Earth initial $^{230}Th/^{232}Th$ atomic ratio of $4.4 \pm 2.2 \times 10^{-6}$. Final ages are given as years before the year 2000 AD (a b2k). Age modelling was performed using StalAge[7], an algorithm specifically designed for speleothems.

Speleothem geochemistry. Trace elements were measured by Laser ablation inductively coupled plasma mass spectrometry (LA-ICPMS) (RESOlution M-50 prototype at RHUL, 193 nm, ArF excimer) with a two-volume LA cell coupled to an Agilent 7500ce quadrupole ICPMS[30] along a ca 8-cm-long profile at the base of the stalagmite (single track). Reported concentrations were calculated following ref. 31 using NIST610 as bracketing external standard and stoichiometric [Ca] of 40% m/m as internal standard.

Sub-samples for $\delta^{18}O$ and $\delta^{13}C$ analyses were milled at 200 µm intervals along the vertical growth axes of the stalagmites using a Merchantek micromill. Analyses of 0.05–0.35 mg calcite powders were performed at the University of Innsbruck on a ThermoFisher Delta^{plus}XL isotope ratio mass spectrometer with an analytical precision (1σ) of 0.08‰ for $\delta^{18}O$ and 0.06‰ for $\delta^{13}C$. Results are reported on the Vienna Pee Dee Belemnite (VPDB) scale and calibrated against NBS19.

The composite 7H-record. The composite 7H $\delta^{18}O$ record (Fig. 4) was obtained using a MC approach applied on absolute age determinations to find the best correlation between adjacent time series (ISCAM[32]). We prescribed a point-wise linear interpolation between data points. The age model was determined from the highest correlation obtained over 100,000 MC simulations using a 50a smoothing. The significance estimation was performed using 2,000 pairs of artificially constructed first-order autoregressive time series (AR1), while each pair was scanned with 1,000 MC simulations to find the best correlation. Finally, the result was re-sampled at annual intervals, detrended and normalized to be compared with other proxy records.

References

1. Clark, P. U. *et al.* The Last Glacial Maximum. *Science* **325,** 710–714 (2009).
2. Hughes, P. D., Gibbard, P. L. & Ehlers, J. Timing of glaciation during the last glacial cycle: evaluating the concept of a global 'Last Glacial Maximum' (LGM). *Earth Sci. Rev.* **125,** 171–198 (2013).
3. Laîné, A. *et al.* Northern hemisphere storm tracks during the last glacial maximum in the PMIP2 ocean-atmosphere coupled models: energetic study, seasonal cycle, precipitation. *Clim. Dynam.* **32,** 593–614 (2009).
4. Hofer, D., Raible, C. C., Merz, N., Dehnert, A. & Kuhlemann, J. Simulated winter circulation types in the North Atlantic and European region for preindustrial and glacial conditions. *Geophys. Res. Lett.* **39,** L15805 (2012).
5. Schneider von Deimling, T., Ganopolski, A., Held, H. & Rahmstorf, S. How cold was the Last Glacial Maximum? *Geophys. Res. Lett.* **33,** L14709 (2006).
6. Ehlers, J. & Gibbard, P. L. *Quaternary Glaciations - Extent and Chronology: Part I: Europe* (Elsevier, 2004).
7. Bini, A. *et al. Switzerland during the Last Glacial Maximum (LGM) 1:500000* (Federal Office of Topography Swisstopo, 2009).
8. Florineth, D. & Schlüchter, C. Alpine evidence for atmospheric circulation patterns in Europe during the Last Glacial Maximum. *Quat. Res.* **54,** 295–308 (2000).
9. Kuhlemann, J. *et al.* Regional synthesis of mediterranean atmospheric circulation during the Last Glacial Maximum. *Science* **321,** 1338–1340 (2008).
10. Jenk, T. M. *et al.* A novel radiocarbon dating technique applied to an ice core from the Alps indicating late Pleistocene ages. *J. Geophys. Res.* **114,** D14305 (2009).
11. Luetscher, M. & Jeannin, P.-Y. Temperature distribution in karst systems: the role of air and water fluxes. *Terra Nova* **16,** 344–350 (2004).
12. Svensson, A. *et al.* The Greenland ice core chronology 2005, 15-42 ka. Part 2: Comparison to other records. *Quat. Sci. Rev.* **25,** 3258–3267 (2006).
13. Rasmussen, S. O. *et al.* A stratigraphic framework for abrupt climatic changes during the last glacial period based on three synchronized Greenland ice core records: refining and extending the INTIMATE event stratigraphy. *Quat. Sci. Rev.* **106,** 14–28 (2014).
14. Bond, G. *et al.* A pervasive millennial-scale cycle in North Atlantic Holocene and Glacial Climates. *Science* **278,** 1257–1266 (1997).
15. Martrat, B. *et al.* Four climate cycles of recurring deep and surface water destabilizations on the Iberian Margin. *Science* **317,** 502–507 (2007).
16. Weinelt, M. *et al.* Variability of North Atlantic heat transfer during MIS 2. *Paleocenanography* **18,** 1071 (2003).
17. Monegato, G. *et al.* Evidence of a two-fold glacial advance during the last glacial maximum in the Tagliamento end moraine system (eastern Alps). *Quat. Res.* **68,** 284–302 (2007).
18. Preusser, F., Graf, H. R., Keller, O., Krayss, E. & Schlüchter, C. Quaternary glaciation history of northern Switzerland. E&G *Quat. Sci. J.* **60,** 282–305 (2011).
19. Wohlfarth, B. *et al.* Rapid ecosystem response to abrupt climate changes during the last glacial period in western Europe, 40–16 ka. *Geology* **36,** 407–410 (2008).
20. Martius, O., Zenklusen, E., Schwierz, C. & Davies, HC. Episodes of Alpine heavy precipitation with an overlying elongated stratospheric intrusion: a climatology. *Int. J. Climatol.* **26,** 149–1164 (2006).
21. Strandberg, G., Brendefelt, J., Kjellström, E. & Smith, B. High-resolution regional simulation of the last glacial maximum climate in Europe. *Tellus* **63A,** 107–125 (2011).
22. Haeberli, W. & Penz, U. An attempt to reconstruct glaciological and climatological characteristics of 18 ka BP ice age glaciers in and around the Swiss Alps. *Z. Gletscherk. Glazialgeol.* **21,** 351–361 (1985).
23. Sodemann, H., Schwierz, C. & Wernli, H. Interannual variability of Greenland winter precipitation sources: Lagrangian moisture diagnostic and North Atlantic Oscillation influence. *J. Geophys. Res. Atm* **113,** D3 (2008).
24. Berger, A. & Loutre, M. F. Insolation values for the climate of the last 10 million years. *Quat. Sci. Rev.* **10,** 297–317 (1991).

25. Huybers, P. Combined obliquity and precession pacing of the late Pleistocene deglaciation. *Nature* **480,** 229–232 (2011).
26. Drysdale, R. N. *et al.* Evidence for obliquity forcing of glacial Termination II. *Science* **325,** 1527–1531 (2009).
27. Huybers, P. Early Pleistocene glacial cycles and the integrated summer insolation forcing. *Science* **313,** 508–511 (2006).
28. Lunt, D. J. & Valdes, P. J. Dust deposition and provenance at the Last Glacial Maximum and present day. *Geophys. Res. Lett.* **29,** 2085 (2002).
29. Shen, C. C. *et al.* High-precision and high-resolution carbonate ^{230}Th dating by MC-ICP-MS with SEM protocols. *Geochim. Cosmochim A* **99,** 71–86 (2012).
30. Müller, W., Shelley, M., Miller, P. & Broude, S. Initial performance metrics of a new custom-designed ArF excimer LA-ICPMS system coupled to a two-volume laser-ablation cell. *J. Anal. Atom. Spectrom.* **24,** 209–214 (2009).
31. Longerich, H. P., Jackson, S. E. & Gunther, D. Laser ablation inductively coupled plasma mass spectrometric transient signal data acquisition and analyte concentration calculation. *J. Anal. Atom. Spectrom.* **11,** 899–904 (1996).
32. Fohlmeister, J. A statistical approach to construct composite climate records of dated archives. *Quatern. Geochron* **14,** 48–56 (2012).
33. Bigler, M. *Hochauflösende Spurenstoffmessungen an Polaren Eisbohrkernen: Glaziochemische und Klimatische Prozessstudien*. PhD thesis, University of Bern 148 (2004).
34. Friedman, I. & O'Neil, J. R. in: *Data of Geochemistry* 6th edn (ed. Fleischer, M.) 1–12 (US Geol. Survey Prof. Paper 440-KK, 1977).

Acknowledgements

M.L. is recipient of an APART-fellowship of the Austrian Academy of Sciences (ÖAW). Partial support by the Austrian Science Fund (FWF, project P222780 to C.S.) is acknowledged. G. Moseley is thanked for providing an additional U/Th age of 7H-3 sample. C. Baroni, W. Haeberli, M. Sarnthein, A. Svensson and H. Wernli are acknowledged for inspiring discussions.

Author contributions

M.L. designed the study, completed the field work together with F.H. and interpreted the results. R.B. carried out the U/Th analyses with support of H.C. and R.L.E. H.S. provided the moisture source analysis; C.S. generated the stable isotope data and contributed to the interpretation together with H.S., S.F. helped in the analysis and interpretation of the speleothem petrography and W.M. carried out the trace element analyses. M.L. wrote the manuscript and designed the figures with input from all co-authors.

Additional information

Supplementary Information accompanies this paper at http://www.nature.com/naturecommunications

Competing financial interests: The authors declare no competing financial interest.

Reprints and permission information is available online at http://npg.nature.com/reprintsandpermissions/

How to cite this article: Luetscher, M. *et al.* North Atlantic storm track changes during the Last Glacial Maximum recorded by Alpine speleothems. *Nat. Commun.* 6:6344 doi: 10.1038/ncomms7344 (2015).

Luetscher, M. et al. *North Atlantic storm track changes during the Last Glacial Maximum recorded by Alpine speleothems. Nat. Commun. 6:6344. doi: 10.1038/ncomms7344 (2015).*

Supplementary Figure 1

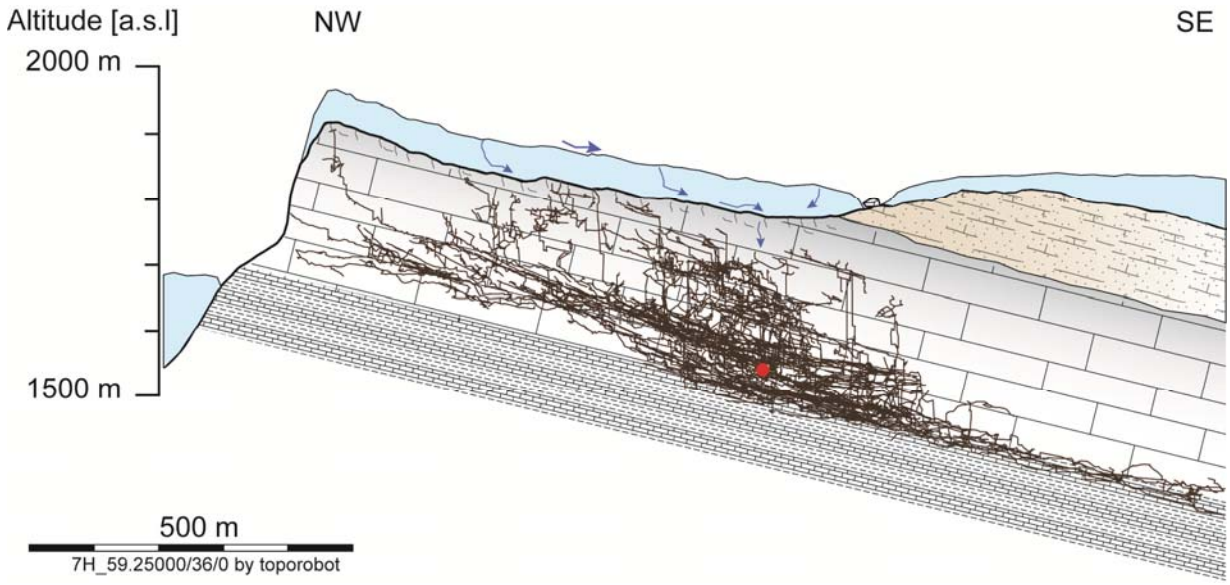

The Sieben Hengste karst system during the Last Glacial Maximum

The Sieben Hengste cave network (here on a vertical cross section) is a complex multiphased speleological system (*1*) located north of Lake Thun, Switzerland. The network comprises more than 157 km of surveyed cave passages, expanding over a surface area of ca. 22 km^2 for a vertical range of 1340 m. The karst aquifer encompasses the 200 m-thick Schrattenkalk Formation (Barremian to Aptian; Urgonian facies, grey shading), a Cretaceous platform limestone formed in the Helvetic realm (*2*). The stratigraphic sequence includes a succession of neritic carbonates comprising chiefly oolithic limestones with variable proportions of dolomite. Bioclasts are mainly present as cm-sized rudists but benthic forams, gastropods and echinodea are also observed (*3*). The geological structure follows a monoclinal slope dipping to the southeast at about 15-30° and is delineated to the east by a large normal fault whose throw reaches up to 1000 m. Low-permeable Eocene sandstones (brown shading) cover part of the surface area above the cave. Between 1700 and 2000 m a.s.l., however, the hydrological catchment chiefly comprises denudated Schrattenkalk characterized by limestone pavements. Erratic boulders and glacial polish point to an ice-covered catchment during the Last Glacial Maximum (blue). Based on observations in the nearby Napf area (4), the equilibrium line altitude during the maximal glacier advance is estimated at ca. 1250 m a.s.l. The LGM-speleothems were sampled in a small alcove at the base of an active vadose shaft, ca. 215 m below the modern ground surface (red dot). The present-day aquifer recharge occurs predominantly during snow melt in spring and during summer storm events. Surface runoff is typically absent in the catchment, but active sinkholes form at the contact with the sandstone draining substantial amounts of water into the underneath karst system. The measured mean annual cave air temperature in this part of the cave system is 4.2±0.1°C and active water infiltration is being observed throughout the year. Modern calcite precipitates from various parts of the cave system yield $\delta^{18}O$ values of -7±1 ‰.

Luetscher, M. et al. *North Atlantic storm track changes during the Last Glacial Maximum recorded by Alpine speleothems. Nat. Commun. 6:6344. doi: 10.1038/ncomms7344 (2015).*

Supplementary Figure 2

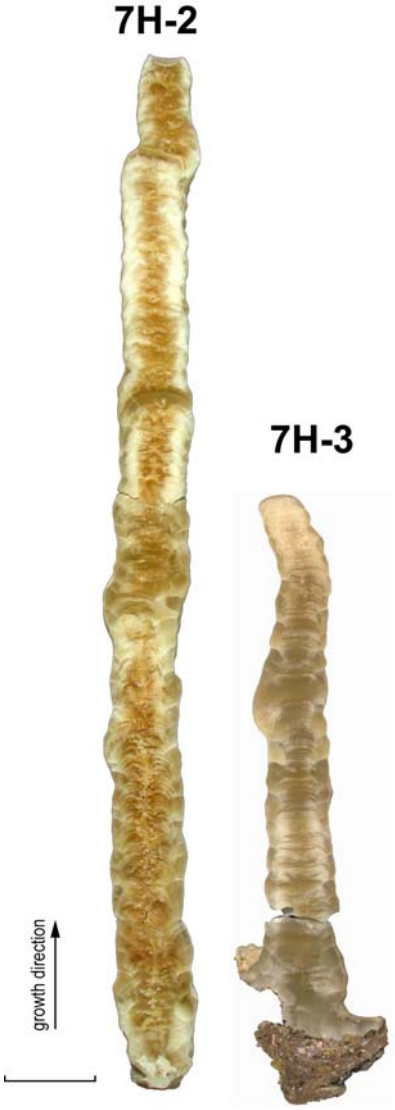

The 7H LGM-speleothems

The two stalagmites were found broken on a collapsed sediment bank. The samples show a similar candle-shaped morphology, which suggests a constant drip rate throughout the period of formation. The absence of significant morphological changes suggests that the mean saturation index (Sicc) must have remained constant throughout the growth history (ca. 0.35 to 0.45 for discharge rates of ca. 0.1 l/day; *5*). The 568 mm-long 7H-2 stalagmite, ca 40 mm in diameter, is honey-coloured. Corrosion features are observed on the outer surface, including a small pool at the drip impact on top of the stalagmite. Approximately 57 mm distance from top (DFT), the growth axis shifted by ca. 10 mm. Age modelling (StalAge; *6*) based on 29 multi-collector MC-ICP-MS U/Th ages associates this shift with a ca. 3ka hiatus but, otherwise, reveals a regular deposition between 30 and 17.2 ka with an average growth rate of 66±27 µm a^{-1} (Supplementary Figure 4). 7H-3 is 302 mm long and shows very similar features to 7H-2 (shape, colour, corrosion patterns). A shift in the growth axis is observed 43 mm DFT likely associated with the subsidence of the fine-grained sediment on which it grew. U/Th ages reveal a very regular growth of 39±11µm a^{-1}, between 22.9 and 14.6 ka, and no sign of a hiatus. Scale bar: 50 mm.

Luetscher, M. et al. *North Atlantic storm track changes during the Last Glacial Maximum recorded by Alpine speleothems. Nat. Commun. 6:6344. doi: 10.1038/ncomms7344 (2015).*

Supplementary Figure 3

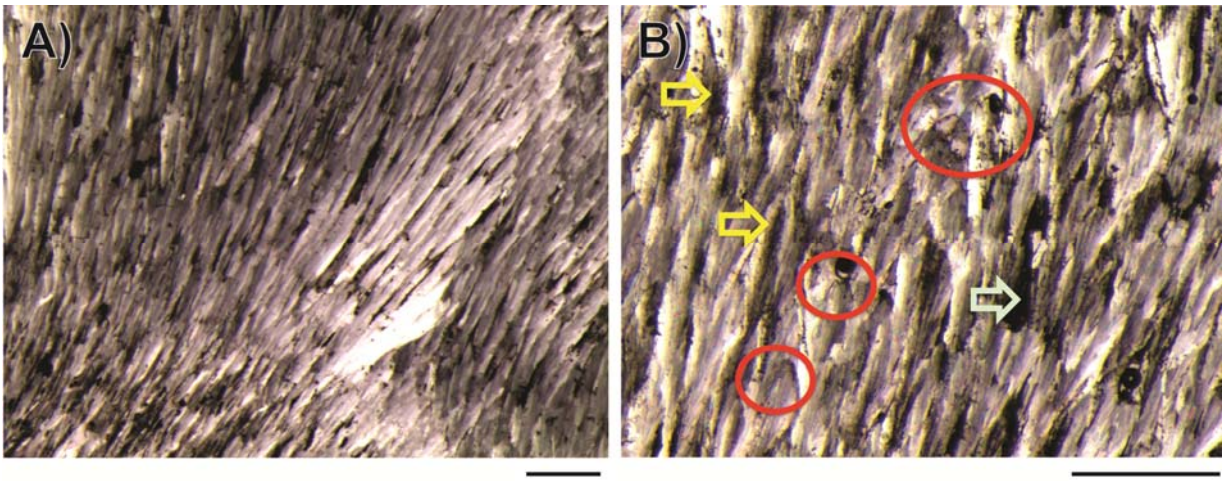

Thin section photomicrographs of 7H stalagmites under crossed polars

The stalagmite petrography is characterized by two types of fabrics comprising bundles of compact and more porous fascicular-optic calcite crystals showing typically divergent optic axes (*7*). Both fabrics indicate that the calcite contains Mg in excess of 1000 ppm (*8*). Fabric (A) consists of close-packed bundles of translucent, elongated columnar, fascicular-optic calcite crystals while fabric (B) is characterized by secondary porosity (greenish arrow) where crystal tips show signs of dissolution followed by reprecipitation of single columnar calcite (red circles). This replacement is associated with more variable hydrology, explaining also the presence of impurities (yellow arrows). Since this early diagenesis occurred prior to, or simultaneous to the deposition of the subsequent layer of fascicular optic bundles, the process has not altered (significantly) the chemical properties of the crystals, and in particular the $\delta^{18}O$ signal, which is believed to reflect that of the parent water. Similar fascicular-optic fabrics have also been observed in cryogenic carbonates (9; 10; 11), which could be associated with microbial oxidation of sulfides present in the host-rock. Microbial oxidation would have likely enhanced dissolution of the bedrock subglacially at low temperature (12) and generated most of the HCO_3^- by the dissolution of the (marine) carbonate rocks, as indicated by the overall positive $\delta^{13}C$ values. Scale bar: 1 mm.

Luetscher, M. et al. *North Atlantic storm track changes during the Last Glacial Maximum recorded by Alpine speleothems. Nat. Commun. 6:6344. doi: 10.1038/ncomms7344 (2015).*

Supplementary Figure 4

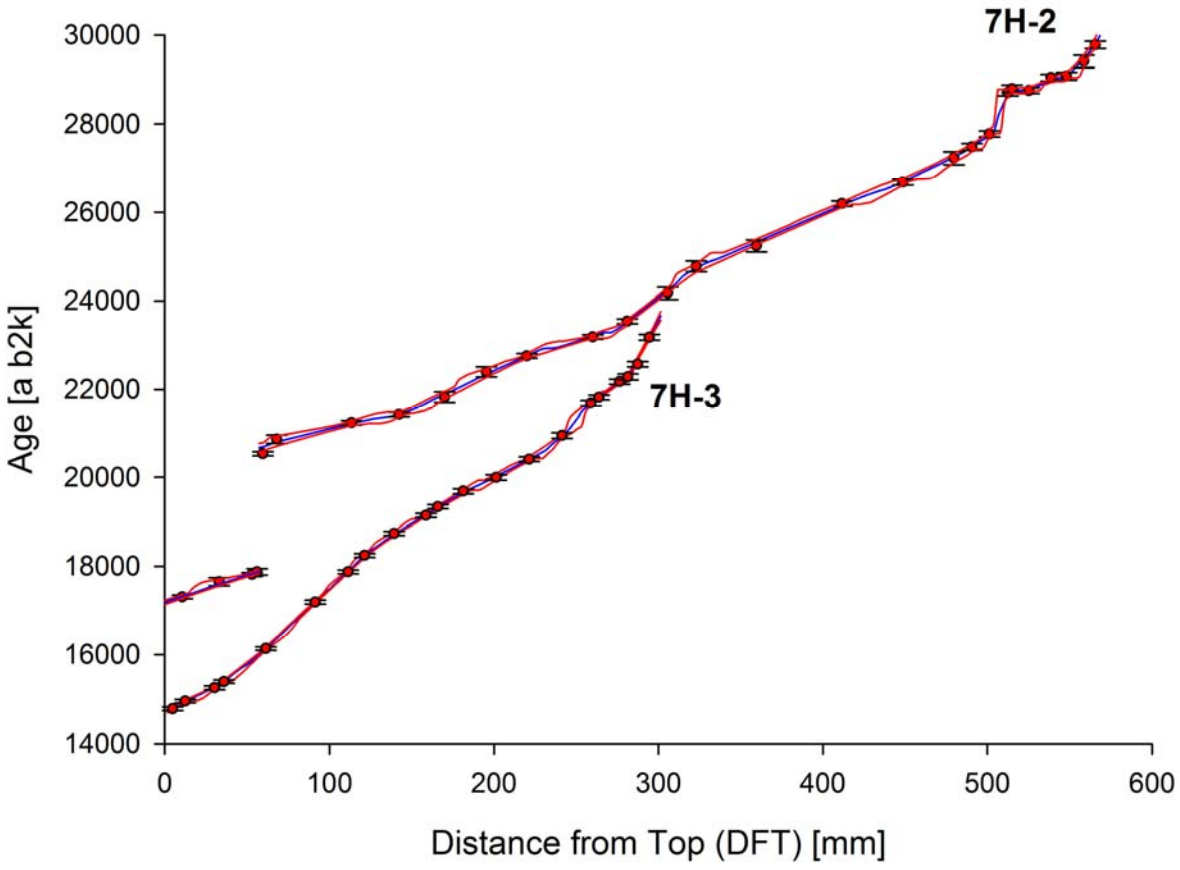

Age model of 7H-2 and 7H-3 stalagmites

Age modelling (StalAge; *6*) reveals rather regular growth rates of 40 to 70 µm a^{-1} on average. Coeval deposition is observed between 23.4 and 20.6 ka as well as between 17.9 and 17.3 ka. A major hiatus identified in 7H-2 between 20.5 and 17.8 ka is supported by petrographical changes showing a shift in the growth axis. In contrast, the absence of clear petrographic evidence for a proper growth stop between 28.7 and 27.8 ka (i.e. during Stadial-4) rather suggests that this period was associated with slow deposition.

Luetscher, M. et al. *North Atlantic storm track changes during the Last Glacial Maximum recorded by Alpine speleothems. Nat. Commun. 6:6344. doi: 10.1038/ncomms7344 (2015).*

Supplementary Figure 5

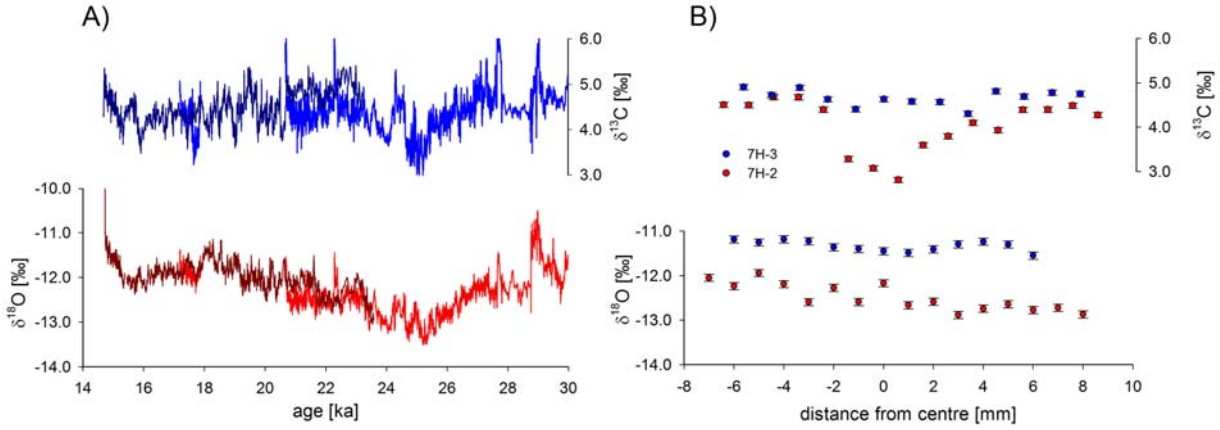

Stable isotope measurements on Sieben Hengste speleothems

A) $\delta^{18}O$ (red) and $\delta^{13}C$ (blue) time series of 7H-2 (bright) and 7H-3 (dark coloured) speleothems. In the overlapping segments, reproducibility is observed between both stalagmites within ±0.6‰ and ±1.0‰ (2σ) for $\delta^{18}O$ and $\delta^{13}C$, respectively. A singular event observed on the 7H-2 $\delta^{18}O$ record between 22.4 and 22.1 ka is, however, not reproduced, suggesting contrasted hydrological responses. This hydrological control is further supported by a significant correlation (r^2=0.54) between $\delta^{13}C$ and $\delta^{18}O$ in 7H-2 which points to a slightly more responsive drip than 7H-3. B) $\delta^{18}O$ and $\delta^{13}C$ analyses along individual growth layers (i.e. Hendy Tests) of 7H-2 and 7H-3. The more positive values observed in 7H-3 suggest that kinetic fractionation affects this sample more strongly. This result is consistent with a somewhat lower drip discharge as inferred from the speleothem growth rate. Overall, the elevated $\delta^{13}C$ values reflect the isotopic composition of the host rock and strongly support the lack of soil-derived organic carbon in the karst system. The higher $\delta^{13}C$ values observed in 7H-3 suggest an early CO_2 degassing associated with a low drip rate.

Luetscher, M. et al. *North Atlantic storm track changes during the Last Glacial Maximum recorded by Alpine speleothems. Nat. Commun. 6:6344. doi: 10.1038/ncomms7344 (2015).*

Supplementary Figure 6

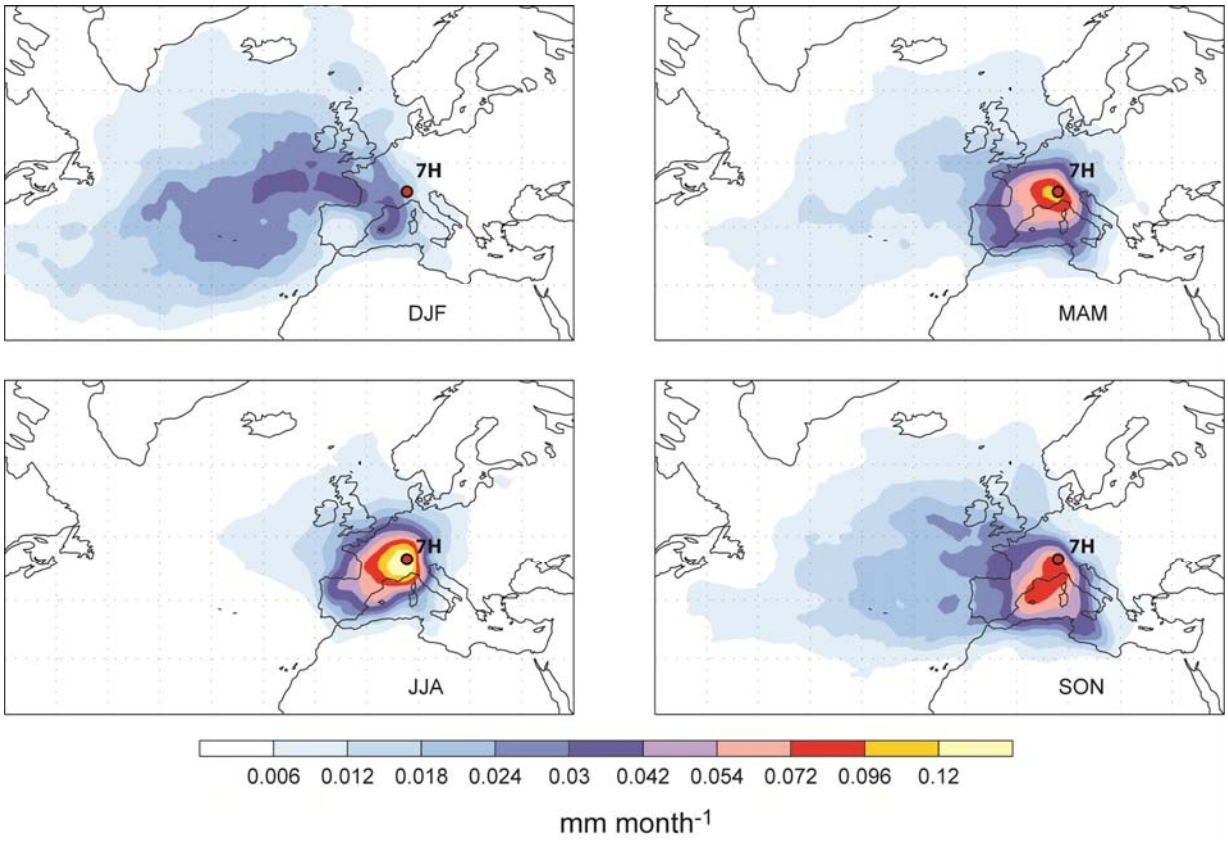

Seasonal mean moisture sources of precipitation reaching the Sieben Hengste

Moisture sources from 1995 to 2005 are expressed as evaporation contribution to total meteoric precipitation at the Sieben Hengste (red dot), in mm month^{-1}.

Luetscher, M. et al. *North Atlantic storm track changes during the Last Glacial Maximum recorded by Alpine speleothems. Nat. Commun. 6:6344. doi: 10.1038/ncomms7344 (2015).*

Supplementary Figure 7

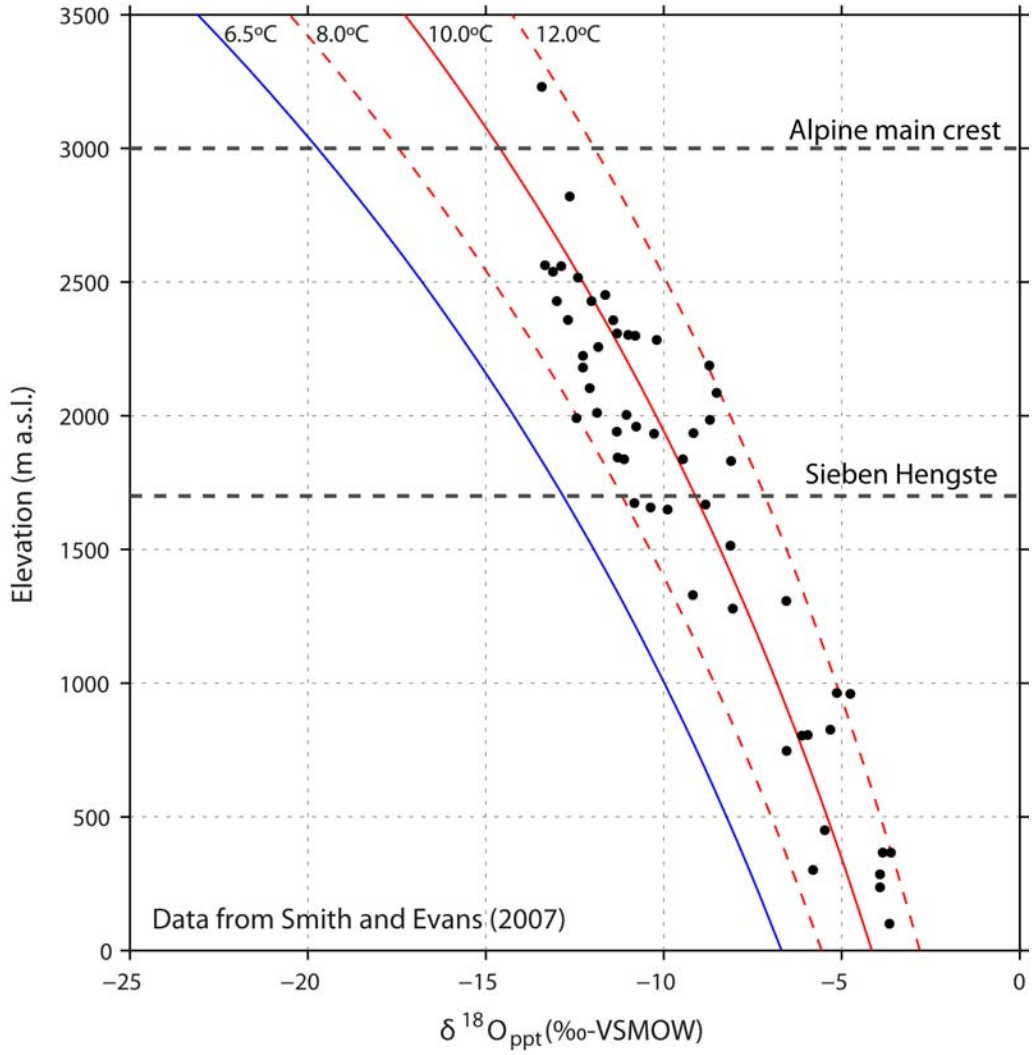

Isotopic depletion in ^{18}O versus barrier elevation

Solid curves are from a Rayleigh fractionation model showing the isotopic composition of precipitation from moisture starting a pseudoadiabatic ascent from a surface temperature of 6.5, 8.0, 10.0 and 12.0°C and a vapour isotope value of -11‰ for δ^{18}O. The presented data (*13*) are best explained by a surface temperature range of 8--12ºC (red lines). For a Rayleigh distillation with a source temperature of 6.5ºC (blue line) a two-member mixing model for the isotopic composition at 7H has been constructed. Elevations of 7H and Alpine main crest are indicated by the horizontal dashed line.

Luetscher, M. et al. *North Atlantic storm track changes during the Last Glacial Maximum recorded by Alpine speleothems. Nat. Commun. 6:6344. doi: 10.1038/ncomms7344 (2015).*

Supplementary Figure 8

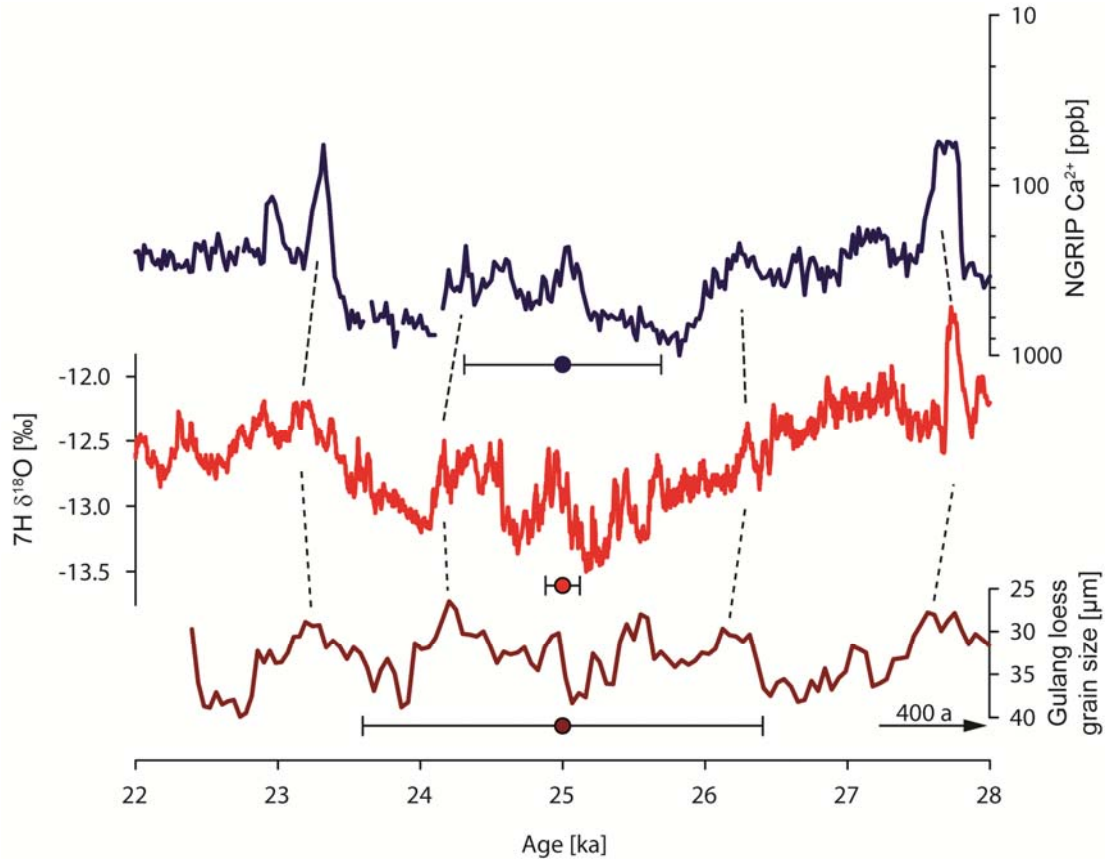

Comparison between 7H and the dust record

The composite 7H $\delta^{18}O$ record (centre), the Greenland dust record (*14*; top) and the Gulang loess record (*15*; bottom) during the Last Glacial Maximum are shown together with their typical age uncertainties (error bars); NGRIP: maximum counting error (2σ; *16*); 7H: U/Th age (2σ); Gulang: OSL age (1σ). The time axis for the Gulang loess record has been offset by 400 a towards older ages to facilitate comparison with the other time series.

Luetscher, M. et al. *North Atlantic storm track changes during the Last Glacial Maximum recorded by Alpine speleothems. Nat. Commun. 6:6344. doi: 10.1038/ncomms7344 (2015).*

Supplementary Table 1

	Mg (m25)	**S (m34)**	**Sr (m88)**	**Ba (m138)**	**U (m238)**
	ppm	ppm	ppm	ppm	ppm
average	7827	460	871	37	1.069
stand. dev.	782	71	163	9	0.323

LA-ICPMS data measured on the 7H-2 sample

The measured trace elements all derive from the dissolution of the marine Schrattenkalk carbonates. The elevated magnesium concentration is consistent with the speleothem petrography, suggesting slow but regular drip rates. The presence of sulphur results from the oxidation of pyrite disseminated in the host rock. This interpretation is consistent with secondary gypsum deposits (δ^{34}S: -32 to -26.3 ‰; *17*), which represent a common feature in the Sieben Hengste cave system. Because sulfide oxidation enhances the dissolution capacity of seepage water, it also represents a major process for speleothem deposition in periglacial karst areas (*18*). It is noteworthy that Y, an element which is commonly associated with colloidal transport from the soil, is largely below detection limit (~13 ppb). No chemical laminations were observed suggesting regular drip chemistry associated with a well-mixed aquifer.

Luetscher, M. et al. *North Atlantic storm track changes during the Last Glacial Maximum recorded by Alpine speleothems. Nat. Commun. 6:6344. doi: 10.1038/ncomms7344 (2015).*

Supplementary Table 2

Sample	DFT (mm)		Isotrack	Lab ID	^{238}U (ppb)	^{232}Th (ppt)	^{230}Th / ^{232}Th (atomic x10^{-6})	$\delta^{234}U$* (measured)	^{230}Th / ^{238}U (activity)	^{238}Th Age (a) (uncorrected)	$\delta^{234}U_{initial}$** (corrected)	^{230}Th Age (a b2K)*** (corrected)
7H2- 8	10.6	±	2.0	RB185	1383.4 ± 1.3	153 ± 4	34880 ± 810	571.0 ± 1.7	0.2334 ±0.0004	17374 ±38	599.7 ± 1.8	**17304 ±38**
7H2- 31	33.0	±	2.0	RB97	1291.8 ± 2.2	304 ± 8	17360 ± 480	640.8 ± 2.5	0.2480 ±0.0010	17662 ±86	673.6 ± 2.6	**17649 ±86**
7H2- 45	53.0	±	2.0	RB186	1170.5 ± 1.2	110 ± 3	43680 ± 1080	636.0 ± 1.9	0.2500 ±0.0010	17884 ±43	668.9 ± 2.0	**17814 ±43**
7H2- 58	56.0	±	2.0	top	1246.8 ± 2.6	286 ±32	17668 ± 1969	612.5 ±2.2	0.2462 ±0.0009	17684 ±74	644.2 ± 2.3	**17672 ±74**
7H2- 51	59.6	±	2.0	RB187	1361.9 ± 1.4	652 ± 13	8060 ± 160	348.6 ± 1.7	0.2340 ±0.0004	20609 ±46	369.4 ± 1.8	**20531 ±47**
7H2- 65	68.0	±	2.0	RB98	1518.4 ± 2.7	355 ± 7	16690 ± 310	347.9 ± 2.3	0.2370 ±0.0010	20870 ±96	369.0 ± 2.5	**20856 ±96**
7H2- 109	113.4	±	2.0	RB188	1416.8 ± 1.6	127 ± 3	44640 ± 1060	356.5 ± 1.8	0.2430 ±0.0004	21302 ±50	378.6 ± 1.9	**21232 ±50**
7H2- 140	142.4	±	2.0	RB205	1537.7 ± 1.8	92 ± 3	67070 ± 1870	355.0 ± 1.8	0.2440 ±0.0010	21491 ±54	377.2 ± 1.9	**21422 ±54**
7H2- 167	170.0	±	2.0	RB123	1489.9 ± 2.4	29 ± 7	208070 ± 51930	361.6 ± 2.6	0.2490 ±0.0010	21830 ±122	384.6 ± 2.8	**21821 ±122**
7H2- 192	195.4	±	2.0	RB99	1382.2 ± 2.8	146 ± 8	40190 ± 2140	376.3 ± 2.8	0.2580 ±0.0010	22410 ±114	400.9 ± 3.0	**22399 ±114**
7H2- 220	220.0	±	2.0	RB206	1763.2 ± 1.9	82 ± 2	96010 ± 2900	423.6 ± 1.7	0.2710 ±0.0010	22828 ±52	451.8 ± 1.8	**22759 ±52**
7H2- 254	260.0	±	2.0	RB189	1420.0 ± 1.4	73 ± 2	88050 ± 2580	412.3 ± 1.7	0.2740 ±0.0004	23257 ±51	440.3 ± 1.8	**23188 ±51**
7H2- 277	281.0	±	2.0	RB242	1373.0 ± 1.4	56 ± 2	110820 ± 3390	401.9 ± 1.8	0.2750 ±0.0004	23609 ±53	429.6 ± 1.9	**23541 ±53**
7H2- 300	305.6	±	2.0	RB124	1026.4 ± 1.5	131 ± 7	35900 ± 2020	385.6 ± 2.6	0.2780 ±0.0010	24182 ±139	412.8 ± 2.8	**24170 ±139**
7H2- 319	323.0	±	2.0	RB100	1415.8 ± 2.6	278 ± 8	24900 ± 720	444.9 ± 2.5	0.2970 ±0.0010	24790 ±123	477.1 ± 2.7	**24777 ±123**
7H2- 354	359.6	±	2.0	RB125	921.6 ± 1.4	208 ± 7	23420 ± 760	530.5 ± 2.9	0.3200 ±0.0010	25251 ±135	569.6 ± 3.1	**25238 ±135**
7H2- 407	411.6	±	2.0	RB190	1032.2 ± 1.0	480 ± 10	11180 ± 230	457.9 ± 1.7	0.3160 ±0.0010	26272 ±58	493.1 ± 1.9	**26195 ±59**
7H2- 443	448.6	±	2.0	RB240	1365.2 ± 1.3	267 ± 6	26470 ± 550	424.7 ± 1.7	0.3130 ±0.0010	26753 ±60	458.0 ± 1.8	**26681 ±60**
7H2- 474	479.6	±	2.0	RB126	1011.2 ± 1.6	391 ± 7	14440 ± 270	512.5 ± 2.9	0.3390 ±0.0010	27244 ±146	553.5 ± 3.1	**27227 ±146**
7H2- 491	490.6	±	2.0	RB308	1149.7 ± 1.7	766 ± 15	8580 ± 170	533.5 ± 2.0	0.3470 ±0.0001	27564 ±76	576.7 ± 2.2	**27483 ±77**
7H2- 500	501.2	±	2.0	RB241	695.8 ± 0.5	735 ± 15	5590 ± 110	564.7 ± 1.9	0.3580 ±0.0010	27865 ±67	610.9 ± 2.1	**27778 ±68**
7H2- 512	512.4	±	2.0	RB416	728.4 ± 0.7	461 ± 10	8039 ± 178	508.4 ± 2.2	0.3541 ±0.0006	28703 ±71	551.3 ± 2.4	**28710 ±71**
7H2- 515	515.0	±	2.0	RB309	1058.1 ± 1.6	284 ± 6	20430 ± 420	413.3 ± 1.9	0.3330 ±0.0010	28871 ±81	448.3 ± 2.0	**28796 ±81**
7H2- 523	525.2	±	2.0	RB207	1415.3 ± 1.4	164 ± 4	46370 ± 1050	390.0 ± 1.7	0.3270 ±0.0010	28828 ±67	423.1 ± 1.8	**28757 ±67**
7H2- 539	538.6	±	2.0	RB417	1519.2 ± 1.8	255 ± 5	32745 ± 679	410.8 ± 1.9	0.3339 ±0.0006	29062 ±74	446.0 ± 2.1	**29049 ±74**
7H2- 548	548.0	±	2.0	RB311	1483.8 ± 2.4	530 ± 11	15490 ± 310	414.2 ± 2.0	0.3360 ±0.0010	29157 ±86	449.7 ± 2.2	**29081 ±86**
7H2- 556	558.6	±	2.0	RB101	1302.2 ± 2.3	313 ± 7	23620 ± 540	436.8 ± 2.7	0.3440 ±0.0010	29430 ±139	474.6 ± 2.9	**29416 ±139**
7H2- 563	565.6	±	2.0	RB208	646.2 ± 0.6	1555 ± 31	2520 ± 50	510.4 ± 1.7	0.3670 ±0.0010	29899 ±74	555.3 ± 1.9	**29786 ±81**
7H2- 566	568.0	±	2.0	base	555.9 ± 1.0	2203 ± 35	1545 ± 25	478.9 ± 2.0	0.3715 ±0.0013	31042 ±135	522.6 ± 2.2	**30958 ±145**
7H3- 3	3.4	±	2.0	RB439	927.5 ± 1.1	107 ± 3	29332 ± 789	609.4 ± 2.3	0.20517 ±0.00044	14748 ±40	635.2 ± 2.4	**14735 ±40**
7H3- 12	11.0	±	2.0	RB300	996.0 ± 1.3	272 ± 6	12577 ± 283	617.5 ± 2.1	0.20852 ±0.00042	14922 ±38	644.1 ± 2.2	**14907 ±38**
7H3- 29	28.8	±	2.0	RB425	1126.7 ± 1.3	68 ± 2	57988 ± 1619	624.3 ± 2.3	0.21329 ±0.00043	15217 ±40	651.7 ± 2.5	**15205 ±40**
7H3- 35	34.8	±	2.0	RB452	962.4 ± 1.1	231 ± 5	14724 ± 307	615.5 ± 2.3	0.21395 ±0.00042	15356 ±40	642.8 ± 2.5	**15341 ±40**
7H3- 60	60.0	±	2.0	RB440	904.8 ± 0.9	107 ± 2	31184 ± 712	621.7 ± 2.1	0.22447 ±0.00041	16096 ±39	650.5 ± 2.2	**16083 ±39**
7H3- 90	90.0	±	2.0	RB426	1236.3 ± 1.4	94 ± 2	50674 ± 1295	588.0 ± 2.2	0.23316 ±0.00042	17150 ±42	617.2 ± 2.3	**17138 ±42**
7H3- 110	110.0	±	2.0	RB482	1025.0 ± 1.1	167 ± 1	24604 ± 200	593.8 ± 2.1	0.24272 ±0.00043	17836 ±43	624.5 ± 2.2	**17822 ±43**
7H3- 120	120.0	±	2.0	RB427	1214.9 ± 1.4	39 ± 1	124142 ± 4740	560.5 ± 2.1	0.24210 ±0.00043	18203 ±44	590.0 ± 2.2	**18191 ±44**
7H3- 138	138.0	±	2.0	RB483	1170.5 ± 1.3	449 ± 2	10139 ± 39	484.6 ± 2.0	0.23600 ±0.00042	18704 ±46	510.8 ± 2.2	**18686 ±46**
7H3- 157	157.4	±	2.0	RB441	1243.9 ± 1.4	65 ± 2	78017 ± 2063	526.4 ± 2.0	0.24755 ±0.00041	19103 ±44	555.6 ± 2.1	**19091 ±44**
7H3- 165	164.6	±	2.0	RB428	1370.9 ± 1.7	23 ± 1	241063 ± 13224	499.0 ± 2.1	0.24532 ±0.00045	19299 ±48	526.9 ± 2.2	**19287 ±48**
7H3- 180	180.0	±	2.0	RB484	1446.9 ± 2.0	104 ± 1	51394 ± 710	353.3 ± 2.3	0.22474 ±0.00047	19649 ±58	373.5 ± 2.4	**19636 ±58**
7H3- 200	200.0	±	2.0	RB442	1749.6 ± 2.4	55 ± 2	120631 ± 3758	353.2 ± 1.9	0.22796 ±0.00057	19958 ±63	373.6 ± 2.1	**19946 ±63**
7H3- 220	220.0	±	2.0	RB429	1712.7 ± 2.2	150 ± 3	43728 ± 996	356.4 ± 1.9	0.23285 ±0.00044	20370 ±52	377.5 ± 2.0	**20357 ±52**
7H3- 240	240.0	±	2.0	RB485	1374.8 ± 2.0	485 ± 2	11299 ± 47	373.4 ± 2.2	0.24156 ±0.00056	20911 ±65	396.1 ± 2.4	**20892 ±65**
7H3- 258	257.6	±	2.0	RB443	1645.3 ± 2.2	136 ± 3	50127 ± 1131	382.3 ± 2.0	0.25096 ±0.00048	21649 ±57	406.4 ± 2.1	**21635 ±57**
7H3- 262	262.4	±	2.0	RB430	1372.4 ± 1.6	42 ± 2	136354 ± 5569	383.9 ± 2.0	0.25263 ±0.00045	21779 ±55	408.2 ± 2.1	**21766 ±55**
7H3- 275	275.0	±	2.0	RB266	1509.7 ± 2.0	286 ± 6	22308 ± 465	381.9 ± 1.8	0.25612 ±0.00049	22143 ±57	406.5 ± 1.9	**22129 ±57**
7H3- 280	280.0	±	2.0	RB486	1451.6 ± 2.2	108 ± 2	57485 ± 934	397.6 ± 2.3	0.26020 ±0.00057	22247 ±67	423.3 ± 2.5	**22235 ±67**
7H3- 286	286.0	±	2.0	GM 315	1066.8 ± 1.0	2260 ± 45	2115 ± 43	439.6 ± 1.7	0.27184 ±0.00044	22580 ±50	468.5 ± 1.8	**22524 ±58**
7H3- 293	293.0	±	2.0	RB444	798.6 ± 0.9	29 ± 2	127748 ± 7217	439.4 ± 2.3	0.27794 ±0.00053	23142 ±64	469.0 ± 2.4	**23130 ±64**

$^{230}Th/^{234}U$ ages of 7H-2 and 7H-3 stalagmites

Analytical errors are at 95% confidence level.

*$\delta^{234}U = ([^{234}U/^{238}U]_{activity} - 1)x1000$.

** $\delta^{234}U_{initial}$ was calculated based on ^{230}Th age (T), i.e., $\delta^{234}U_{initial} = \delta^{234}U_{measured} \times e^{\lambda 234 \times T}$.

Following decay constants were used: $\lambda^{230} = 9.158 \times 10^{-6}$ a^{-1} (19); $\lambda^{234} = 2.826 \times 10^{-6}$ a^{-1} (19); $\lambda^{238} = 1.551 \times 10^{-10}$ a^{-1} (20). Corrected ^{230}Th ages assume an initial $^{230}Th/^{232}Th$ atomic ratio of 4.4±2.2 x10^{-6}; i.e. values in secular equilibrium with a bulk Earth $^{232}Th/^{238}U$ value of 3.8. The errors are arbitrarily assumed to be 50%.

*** a b2k stands for before 2000 AD.

Luetscher, M. et al. *North Atlantic storm track changes during the Last Glacial Maximum recorded by Alpine speleothems. Nat. Commun. 6:6344. doi: 10.1038/ncomms7344 (2015).*

Supplementary Discussion

The modern annual precipitation at the study site averages 2000 mm, nearly 40% of which fall as snow between November and April. The $\delta^{18}O$ of precipitation typically averages -13.1±0.6 ‰-VSMOW with a seasonal amplitude of ca. 10 ‰ (*21*). 10-day backward trajectories calculated from an ERA-Interim reanalysis data for the years 1995-2005 were started at 6 hours intervals on a 60x60 km horizontal grid with 30 hPa vertical intervals. A quantitative Lagrangian moisture source diagnostic (*22, 23*) reveals a dominant transport direction from the West, which is particularly pronounced during the winter season (Supplementary Figure 6). However, a seasonally varying fraction of moisture ranging on average between 10 and 30 % also reaches the 7H site from the South. Our method underestimates the seasonal variability since convective (summer) precipitation is less reliably captured. From climatological studies based on precipitation measurements, it is known that about 1/3 of the precipitation along the Northern Alps falls during the summer season, with the remaining 2/3 distributed equally over the other seasons (24).

While Mediterranean moisture sources can contribute substantial amounts of precipitation to the southern Alps during spring and autumn, cluster analyses of extreme rainfall events in northwestern Italy suggest that the strongest precipitation events are likely associated with significant moisture advection from the North Atlantic during periods of intense northward flow to the southern Alpine range (*25*). An increasing number of studies provide evidence that the North Atlantic is the dominant oceanic moisture source of alpine precipitation also in periods of strong southerly moisture advection (*26*). Considering drying ratios as low as 35 % (*27*) a substantial amount of North Atlantic sourced moisture may eventually reach the Sieben Hengste, also with southerly transport routes.

The ^{18}O depletion associated with orographic precipitation depends predominantly on thermodynamic effects (*28*) with topography being the dominant control on the isotope ratio of precipitation. Empirical observations from the Andes (*13*) confirm that $\delta^{18}O$ values largely follow a Rayleigh fractionation model with a mean gradient of ca. 3-4 ‰ per 1000 m barrier elevation (Supplementary Figure 7). Considering all other parameters equal and assuming an average topographic barrier south of the study site at ca. 3000 m a.s.l., the potential difference in the $\delta^{18}O$ signal associated with southerly advection reaches 5 to 7 ‰ as compared to the direct route from the North-West. Using the Rayleigh fractionation model a two end-member mixing model has been constructed for different surface temperatures. Given the approximate 50% threshold value at 16.3‰ $\delta^{18}O$-VSMOV (Figure 4), a best matching mixing model was obtained with end-member values of 19.7‰ for the Alpine main crest and 12.8‰ for the direct approach to 7H, based on an initial surface temperature of 6.5ºC. This transfers the $\delta^{18}O$ signal of between 1.5 and 3 ‰ as inferred from the peak glacial $\delta^{18}O$ shift in the 7H-record to a southern humidity fraction ranging from 25 to 65 % of the average annual precipitation at Sieben Hengste during the LGM. Sensitivity of the estimate is about 10% less southerly contribution per degree in surface temperature change.

In contrast to the storm trajectories, local temperature effects are assumed to play only a second order role in the isotope fractionation affecting meteoric precipitation reaching the Sieben Hengste. Changing the temperature of condensation is expected to produce comparatively small amplitudes in isotope fractionation on palaeoclimate timescales. Typically, major precipitation events go along with substantial advection of warm moist air, which, due to its transient nature, is hardly reflected in the mean annual air temperature record. For example, temperature of precipitation in Greenland is up to 15 K warmer than the annual mean temperatures (22).

From present-day synoptic analysis it is well known that events of heavy precipitation in the Southern Alps are typically associated with intense moisture advection from the North Atlantic, in some cases tapping into the subtropical pool of high humidity (*25*). Such cases of meridional moisture advection are typically associated with a trough signature at mid-tropospheric levels, also known as narrow potential vorticity streamers. The jet stream bends around the outside of these troughs (streamers), and induces the dominant transport pattern in the troposphere below. When the Fennoscandian ice cap was present during the LGM, atmospheric motion was different as compared to today, (i) by a equatorward shift of the sea-ice margin, and thus the zone for baroclinic storm development, and (ii) by inducing a frequent cold high-pressure residing over the ice cap, blocking the flow and deflecting the jet stream, inducing pronounced undulations, known as Rossby wave breaking. With the tropics (and subtropics) cooling less

than high-latitudes during the LGM, substantial moisture should have been available in proximity to the equatorward shifted baroclinic zone (storm track) and the overlying jet stream. As the disturbances due to the blocking anticyclone not just die off, but can continue to influence weather downstream, it is possible that additional wave breaking was induced over central and eastern Asia, triggering again strong meridional advection patterns underneath upper-level jet excursions. This time the systems would not transport moisture towards the Alps, but generate storms that could transport large amounts of dust into higher (Arctic) latitudes. Additional or alternative mechanisms may have included (i) increased deflation of aeolian material in the dust sources, (ii) increased wind speed due to changed land cover, (iii) larger deserts, (iv) less effective removal processes, (v) a more direct transport pathway towards the Arctic.

Supplementary References

1. Häuselmann, P., Jeannin, P.-Y. Sieben Hengste, Switzerland. In Gunn (ed.), Encyclopedia of Caves and Karst Science, Fitzroy Dearborn, 647-649 (2004).
2. Pfiffner, O.A. Structural Map of the Helvetic Zone of the Swiss Alps, including Vorarlberg (Austria) and Haute Savoie (France), 1:100 000.*Geological Special Map*, **128**. Explanatory notes (2011).
3. Ziegler, M.A. A study of the Lower Cretaceous facies developments in the Helvetic Border Chain, north of the Lake of Thun (Switzerland). *Eclog. Geologic. Helvet.,* **60**, 509-527 (1967).
4. Bini, A., Buoncristiani, F., Couterrand, S., Ellwanger, D., Fleber, M., Florineth, D., Graf, H.R., Keller, O., Kelly, M., Schlüchter, C., Schoeneich, P. Switzerland during the Last Glacial Maximum (LGM) 1:500000. Federal Office of Topography Swisstopo, Switzerland. (2009).
5. Miorandi, R., Borsato, A., Frisia, S., Fairchild, I.J., Richter, D.K. Epikarst hydrology and implications for stalagmite capture of climate changes at Grotta di Ernesto (NE Italy): results from long-term monitoring. *Hydrol. Process.*, **24**, 3101-3114 (2010).
6. Scholz, D., Hoffmann, D.L. StalAge An algorithm designed for construction of speleothem age models. *Quat. Geochronology.*, **6**, 369-382 (2011).
7. Kendall, A.C. Fascicular-optic calcite – replacement of bundled acicular carbonate cements. *J. Sedim. Petrol.*, **47**, 1056-1062 (1977).
8. Frisia, S., Borsato, A.. Karst. In A.M. Alonso-Zarza and L.H. Tanner (eds), Carbonates in Continental Settings: Facies, Environments, and Processes Developments in Sedimentology. Elsevier, 269–318 (2010).
9. Richter, D.K., Riechelmann, D.F.Ch. Late Pleistocene cryogenic calcite spherolites from the Malachitdom Cave (NE Rhenish Slate, Mountains, Germany): origin, unusual internal structure and stable C-O isotope composition, *Int. J. Speleology*, **37**, 119-129 (2008).
10. Žák, K., Onac, B., Perşoiu, A. Cryogenic carbonates in cave environments: A review. *Quat.Int.*, **187**, 84-96 (2008).
11. Luetscher, M., Borreguero, M., Moseley, G., Spötl, C., Edwards, L.E.. Alpine permafrost thawing during the Medieval Warm Period identified from cryogenic cave carbonates. *The Cryosphere*, **7**, 1073-1081 (2013).
12. Mitchell, A.C., Brown, G.H., Modeling geochemical and biogeochemical reactions in subglacial environments. *Arct. Antarct. Alp. Res.*, **40**, 531-547 (2008).
13. Smith, R.B., Evans, J.P. Orographic precipitation and water vapour fractionation over the Southern Andes. *J. Hydrometeorology*, **8**, 3-19 (2007).
14. Bigler, M. Hochauflösende Spurenstoffmessungen an polaren Eisbohrkernen: Glaziochemische und klimatische Prozessstudien. PhD, University of Bern, Switzerland, 148 p. (2004).
15. Sun, Y., Clemens, S.C., Morrill, C., Lin, X., Wang, X., An, Z., Influence of Atlantic meridional overturning circulation on the East Asian winter monsoon. *Nature Geosci.* **5**, 46-49 (2012).
16. Andersen, K.K., Svensson, A., Johnsen, S.J., Rasmussen, S.O., Bigler, M., Röthlisberger, R., Ruth, U., Siggaard-Andersen, M.L. Steffensen, J.P., Dahl-Jensen, D., Vinther, B.M., Clausen, H.B. The Greenland ice core chronology 2005, 15-42 ka. Part 1: constructing the time scale. *Quat. Sci. Rev.*, **25**, 3246-3257 (2006).
17. Filipponi, M. Spatial Analysis of Karst Conduit Networks and Determination of Parameters Controlling the Speleogenesis along Preferential Lithostratigraphic Horizons. PhD Thesis, Ecole Polytechnique Fédérale de Lausanne.

18. Luetscher, M., Hoffmann, D., Frisia, S., Spötl, C. Holocene glacier history from alpine speleothems, Milchbach cave, Switzerland. *Earth Plan. Sci. Lett.*, **302**, 95–106 (2011).

19. Cheng, H., Edwards, R.L., Hoff, J., Gallup, C.D., Richards, D.A., Asmerom, Y., 2000. The half-lives of uranium-234 and thorium-230, *Chem. Geol.* **169**, 17-33 (2000).

20. Jaffey, A.H., Flynn, K.F., Glendenin, L.E., Bentley, W.C., Essling, A. M., Precision measurement of half-lives and specific activities of 235U and 238U. *Phys. Rev*. **C4**, 1889–1906 (1971).

21. Schürch, M., Kozel, R., Schotterer, U., Tripet, J.-P. Observation of isotopes in the water cycle -the Swiss National Network (NISOT). *Environm. Geol.*, **45**, 1–11 (2003).

22. Sodemann, H., Schwierz, C.; Wernli, H., 2008. Interannual variability of Greenland winter precipitation sources: Lagrangian moisture diagnostic and North Atlantic Oscillation influence. *J. Geophys. Res. Atm.*, **113**, D3 (2008).

23. Sodemann, H., Zubler, E. Seasonal and inter-annual variability of the moisture sources for Alpine precipitation during 1995-2002. *Int. J. Climatol.*., **30**, 947–961 (2010).

24. Frei, C, Schär, C. A Precipitation climatology of the Alps from high-resolution rain-gauge observations. *Int. J. Climatol.,* **18**: 873–900 (1998).

25. Pinto, J.G., Ulbrich, S., Parodi A., Rudari R., Boni G., Ulbrich U. Identification and ranking of extraordinary rainfall events over Northwest Italy: The role of Atlantic moisture, *J. Geophys. Res. Atmos.*, **118**, 2085–2097, doi:10.1002/jgrd.50179 (2013).

26. Winschall, A., Sodemann, H., Pfahl, S., Wernli, H., How important is intensified evaporation for Mediterranean precipitation extremes? *J. Geophys. Res. Atmos.*, **119**, 5240–5256, doi:10.1002/2013JD021175 (2014).

27. Smith, R.B., Jiang, Q., Fearon, M.G., Tabary, P., Dorninger, M., Doyle, J.D., Benoit, R. Orographic precipitation and air mass transformation: an Alpine example. *Q.J.R. Meteorol. Soc.*, **129**, 433-454 (2003).

28. Stern, L.A., Blisniuk, P.A. Stable isotope composition of precipitation across the southern Patagonian Andes. *J. Geophys. Res. Atm.*, **107**, D23 (2002).